Single-Cell Acoustic Force Spectroscopy (scAFS): Resolving kinetics and strength of T-cell adhesion to fibronectin

Douwe Kamsma, Pascal Bochet, Felix Oswald, Nander Ablas, Sophie Goyard, Gijs J L Wuite, Erwin J.G. Peterman, Thierry Rose

▶ **To cite this version:**

Douwe Kamsma, Pascal Bochet, Felix Oswald, Nander Ablas, Sophie Goyard, et al.. Single-Cell Acoustic Force Spectroscopy (scAFS): Resolving kinetics and strength of T-cell adhesion to fibronectin. Cell Reports, 2018, 24 (11), pp.3008-3016. 10.1016/j.celrep.2018.08.034 . pasteur-02361962

HAL Id: pasteur-02361962
https://pasteur.hal.science/pasteur-02361962

Submitted on 13 Nov 2019

HAL is a multi-disciplinary open access archive for the deposit and dissemination of scientific research documents, whether they are published or not. The documents may come from teaching and research institutions in France or abroad, or from public or private research centers.

L'archive ouverte pluridisciplinaire **HAL**, est destinée au dépôt et à la diffusion de documents scientifiques de niveau recherche, publiés ou non, émanant des établissements d'enseignement et de recherche français ou étrangers, des laboratoires publics ou privés.

Single-Cell Acoustic Force Spectroscopy (scAFS): Resolving kinetics and strength of T-cell adhesion to fibronectin

Authors: Douwe Kamsma[1,2,6], Pascal Bochet[3,4,6], Felix Oswald[5], Nander Ablas[1,2], Sophie Goyard[3], Gijs J L Wuite[1,2,7,*], Erwin J G Peterman[1,2,7,*], Thierry Rose[3,7,*].

Affiliations :

[1]Department of Physics and Astronomy, Vrije Universiteit Amsterdam, Amsterdam, The Netherlands.
[2]LaserLaB Amsterdam, Vrije Universiteit Amsterdam, Amsterdam, The Netherlands.
[3]Institut Pasteur, Center for Innovation and Technological Research, Networks & Signaling research group, Paris, France.
[4]CNRS UMR3691, Dynamique Cellulaire Physiologique Pathologique, Paris, France.
[5]LUMICKS b.v., Amsterdam, the Netherlands.
[6]These authors contributed equally to this work.
[7]These authors acted as the senior authors of this research.
*Correspondence : G.J.LW. (g.j.l.wuite@vu.nl), E.J.G.P. (e.j.g.peterman@vu.nl) and T.R. (rose@pasteur.fr); ORCID ID 0000-0001-8863-0207)

KEYWORDS

scAFS, single-cell, acoustic force spectroscopy, adhesion strength, adhesion kinetics, CD4, T-lymphocytes, fibronectin, integrin, ECM, extracellular matrix, rupture force, mechanobiology

SUMMARY

Assessing strength and kinetics of molecular interactions of cells with the extracellular matrix is fundamental to understand cell-adhesion processes. Given the relevance of these processes, there is a strong need for physical methods to quantitatively assess the mechanism of cell adhesion at the single-cell level, allowing discrimination of cells with different behaviours. Here we introduce single-cell Acoustic Force Spectroscopy (scAFS), an approach that makes use of acoustic waves to exert controlled forces, up to 1 nN, to hundreds of individual cells in parallel. We demonstrate the potential of scAFS by measuring adhesion forces and kinetics of $CD4^+$ T-lymphocytes (CD4) to fibronectin. We determined that CD4 adhesion is accelerated by interleukin-7, their main regulatory cytokine, while CD4 binding strength remains the same. Activation of these cells likely increases their chance to bind to the vessel wall in the blood flow to infiltrate inflamed tissues and locally coordinate the immune response.

INTRODUCTION

Cell adhesion to the extracellular matrix (ECM) is not only central to tissue assembly and repair, but also to immune surveillance and response (Ley et al., 2007). Adhesion kinetics and strength are currently measured with atomic force microscopy (AFM) (Benoit et al., 2000; Lehenkari and Horton, 1999; Li et al., 2003), surface plasmon resonance technology (SPR) (Kim et al., 2011), fluid-flow devices (Lu et al., 2004), shear-spinning disks (Boettiger, 2007; Friedland et al., 2009; Garcia et al., 1998), centrifugation methods (Reyes and Garcia, 2003) or micropipette aspiration (Hogan et al., 2015) . Accurate measurements of cell-adhesion kinetics and strength absolutely require large and well-defined datasets, in order to grasp the heterogeneity in cell behavior of cell subsets and to capture rare events. Here we present a massively

parallel approach that allows such accurate force control while continuously monitoring many cells using optical microscopy.

It has been shown that acoustic forces can be applied directly to manipulate cells (Marx, 2015) or for flow-sorting purposes according to their density (Laurell et al., 2007) or their size (Petersson et al., 2007). Recently, we presented acoustic force spectroscopy (AFS) as a new single-molecule method to apply well-controlled forces up to hundreds of pN to single (bio)molecules with standing acoustics waves, using microspheres as force transducers (Sitters et al., 2015). Here we show that cells have by themselves enough acoustic contrast such that forces on the order of nN can be applied to them directly, allowing accurate determination of their interactions with the ECM. We call this method single-cell acoustic force spectroscopy (scAFS).

scAFS is performed in a transparent microfluidic flow chamber that can be combined with any optical microscope (**Figure S1**). Well-controlled high forces in the nN range can be applied to hundreds of cells in parallel with scAFS, while tracking their positions in three dimensions in real time. We demonstrate the potential of scAFS by measuring the adhesion process of human primary $CD4^+$ T-lymphocytes (CD4). In the human body, CD4 escape the blood stream upon activation, bind to the blood-vessel endothelial cells near inflamed areas, migrate through the endothelium and infiltrate inflamed or infected tissues as illustrated in **Figure 1** (Butcher, 1991; Ley et al., 2007; Schnoor et al., 2015; Springer, 1994). Integrins expressed on CD4 are inactive in their resting state and numerous studies describe their increased adhesion upon stimulation with various antigens, chemokines and cytokines (Dustin and Springer, 1989; Kinashi, 2012). Here, we quantify the effect of Interleukin-7 (IL7) activation (Cimbro et al., 2012; Kondrack et al., 2003; Mazzucchelli and Durum, 2007; Tamarit et al., 2013) on the binding kinetics and strength of CD4 to fibronectin, a major component of the ECM targeted by integrins (Garcia et al., 1998; Li et al., 2003). This simplified model of CD4 adhesion serves as a testbed to demonstrate the capabilities of scAFS in quantitative studies of cell adhesion.

RESULTS

Manipulating cells with acoustic forces

In our scAFS experiments, the flow chamber is coated with fibronectin, commonly used to mimic the ECM or integrin targets lining the endothelium of blood vessels (**Figure S1**). CD4, purified from healthy donor blood samples, are injected into the AFS chamber and allowed to settle down on the fibronectin-functionalized bottom surface (**Figure 2A,B**). Subsequently, a standing acoustic wave is generated in the flow chamber. The acoustic frequency defines the position of the nodal plane, while the amplitude determines the magnitude of the acoustic force. When acoustic force is applied, unbound cells move towards the nodal plane, while adherent cells remain attached to the surface (**Figure 2C,D**). Unbound and adherent cells can be discriminated on the basis of their diffraction patterns in a bright-field microscopy image, which changes when a cell moves away from the optical focal plane (**Figure 2D,E**). The position of each cell can be determined from its diffraction pattern in real time in three dimensions, using quadrant interpolation (van Loenhout et al., 2012) and a look-up table (Sitters et al., 2015), with an accuracy of 2.0 nm in x and y, and 72 nm in z (**Figure S2**). Given that only µm-scale observations are required for the experiments presented here, this accuracy provides a large margin for inaccuracies due to changes in cell shape. In a typical experiment, an acoustic force of ~10 pN is applied for ~2 s, the minimal force required to push unbound cells upward to the nodal plane. Subsequently, the force is switched off and the cells sediment back to the bottom glass surface (**Figure 2G**). For unbound cells, substantial movements are observed in the xy-plane (**Figure 2F**), due to free diffusion and weak acoustic pressure deviations in this

plane (Spengler, 2003), as can be observed in **Figure S3A**. In contrast, the *xy*- and *z*-positions of bound cells remain unchanged. These results demonstrate that, with scAFS, force can be applied to the cells, while tracking their individual positions in the field of view (in our instrument: 1.8 mm^2), allowing detailed investigation of their adhesion to the fibronectin-functionalized surface.

Three binding stages of adhering cells

In order to quantify the kinetics of CD4 adhesion to fibronectin, we apply a minimal acoustic pulse every two minutes, 9 times in a row, while continuously imaging the cells. From the images, cells are identified and selected automatically. Clustered cells are excluded after visual inspection. Using this approach, we typically track several hundreds of cells simultaneously in three dimensions. Three populations of cells are distinguished based on their *xyz*-trajectories (**Figure 3**): "unbound", "binding" and "bound" cells. Unbound cells move upward each time an acoustic force is applied, indicating that they are not bound to fibronectin. These cells move substantially in *x* and *y* when elevated by the acoustic force and some can shift more than others due to the weak local lateral acoustic pressure deviations. Binding cells show substantial shifts in the *xy*-plane along the bottom surface (1-3 μm), without moving in the *z*-direction. These cells appeared to be crawling, in the process of adhering, but not completely immobilized yet. Bound cells do not move upward upon acoustic-force application and shift only minimally in the *xy*-plane (<1 μm). Based on these observations, we use *xy*-shifts of 1 and 3 μm as boundary values to classify the cells in the three categories.

IL7 accelerates CD4 adhesion

To further assess the progression from unbound to bound cells, we measure the adhesion status of cells with a minimal acoustic pulse at 5, 20, 40 and 60 minutes after cell injection in the AFS chamber. Applying only four acoustic pulses minimizes the perturbation of the cell-adhesion process. **Figure 4A** shows superimposed image pairs before and after the acoustic pulse for non-activated and IL7-activated CD4 after 20 minutes of incubation (see **Figure S3** for 5, 40 and 60 min). Whisker plots in **Figure 4B** display the *xy* shifts of these cells 20 minutes after injection under different conditions. Addition of peptide inhibitors, which targeting the integrins binding fibronectin through its RGD motif (Bernhagen et al., 2017), results in substantially decreased binding of cells to the fibronectin surface (**Figure 4D**). In the absence of fibronectin no adhesion of cells is observed (**Figure 4B**). These observations confirm that adhesion is mediated by integrin-fibronectin interactions**.** In the presence of fibronectin, IL7 activation increases by 44% the fraction of immobilized cells from 27% to 39% (**Figure 4B**). To illustrate the progression of cell binding, the shifts in *xy*-position of the cells are plotted as a cumulative distribution function (CDF) (**Figure 4C**). CDFs show the three cell subsets described above: bound, binding and unbound cells. The percentages of cells in the bound state are plotted at different time points, in the presence or absence of IL7 activation (**Figure 4E**). These results show that the fraction of bound cells increases with incubation time. While two thirds of the cells are bound after 60 minutes independently of their activation status, the adhesion process is substantially faster for IL7-activated CD4.

Calibration of the acoustic force acting on the cells

Determining the binding strength of CD4 to fibronectin-functionalized surface requires calibration of the acoustic forces acting on the cells. Since cells vary substantially in size, density and stiffness, it is imperative to calibrate the forces acting on a representative number of cells. To this end, we measured the Stokes' drag force from the upward velocity (in the *z* direction) of each CD4 when pushed towards the acoustic nodal plane. Buoyancy and gravity acting on the cells can be calculated independently based on their size and weight. The acoustic force is in balance with these three forces and can thus be determined for each

individual cell (Kamsma et al., 2016) (**Figure S4**). Cell velocities are measured during application of successive acoustic pulses of increasing amplitude, spaced by ~1 minute to allow the cells to sediment back to the bottom of the AFS chamber (**Figure 5A**). The cells' upward velocity (slope at the inflexion point) during acoustic pulses increases with the acoustic amplitude, while the cell sedimentation velocity stays the same (**Figure 5B**). From these data, we calculated the force acting on each cell as a function of the amplitude of the electric voltage (V_{pp}) applied to the piezoelectric element and obtained quadratic scaling in accordance with theory (Settnes and Bruus, 2012). We compared the calibration for IL7-activated and non-activated cells from different donors and found that the calibration is indeed similar (**Figure 5C**).

Binding strength of unbound, binding and bound CD4

In order to measure the adhesion strengths to fibronectin of CD4, we applied a voltage ramp. We calibrated the forces acting on each cell during the ramp using calibration parameters obtained from separated measurements on a subset of cells (**Figure 5C**). In such an experiment we observe that most bound cells show an elevation in two steps (**Figure 5D**). In the first step, the cells are elevated by less than 2 μm without moving in the *xy*-plane. In the second step, these cells are elevated to the acoustic node and also move substantially in the *xy*-plane (**Figure S5D,F**). We interpret the first step as either an extension of fibronectin fiber or a deformation of the cells which remain bound to the fibronectin-coated surface, and the second step as the actual rupture of fibronectin-integrin bonds (**Figure 5D**). This method to measure the force causing bond rupture is detailed in **Figure S5.** We note that rupture force is defined here as the force at which the last interaction between cell and fibronectin breaks and the cell moves up from the surface. In order to demonstrate that the fibronectin is not detaching from the surface during the application of acoustic force, we covalently attach microspheres to the fibronectin and observe that all microspheres remain attached after applying 500 pN (**Figure 5E**). The maximal observed extension of glass-adsorbed fibronectin is 150 nm, with a resolution of 72 nm in the *z* direction.

Before measuring CD4 rupture forces, we determined whether cells were unbound, binding or bound by repeatedly applying minimal force pulses. Then we applied a linear force ramp and determined at what force each cell ruptures from the fibronectin-coated surface (**Figure S5F**). Box plots of the rupture forces are clearly different for the three classes of cells (**Figure 6A**), with median values of 9, 39 and 100 pN (unbound, binding and bound, respectively) for non-activated and 15, 39 and 112 pN for IL7-activated cells. The distributions of rupture forces show clear overlap for the three subsets (**Figure 6C**) an**d** are similar from one blood donor to another (**Figure S6**). The binding strength is not affected by IL7-activation, while, as a result of the faster binding kinetics (**Figure 4E**), the proportion of bound cells is increased (**Figure 6B**).

DISCUSSION

We have resolved the adhesion strength and kinetics of individual CD4 binding to fibronectin. Three classes of cells could be distinguished: unbound, binding and bound. Interaction strengths were below 30 pN for unbound cells, below 55 pN for transient binding and crawling cells, and from 55 to hundreds of pN for bound cells. In AFM experiments the average rupture force of a single integrin-fibronectin bond has been shown to be ~40 pN at a loading rate of 20 pN/s (Li et al., 2003). This single-bond rupture force suggests that the unbound, binding, or bound cells that we characterized were held by zero, one, or several integrin bonds, respectively. The adhesion strength was not affected by IL7-activation, but adhesion kinetics was. This accelerated kinetics could be necessary for the cells to resist the shear force (~150 pN) due to the blood flow challenging cell adhesion. The shear force is about four times the strength of a single integrin-fibronectin bond, which suggests that IL7 triggers the inside-out integrin activation pathway, resulting in faster binding kinetics. Nevertheless, the slower, but same-strength outside-in integrin activation pathway

is still available for non-activated cells not experiencing shear stress. In capillaries, 1800-2000 CD4 per microliter of blood are carried by a flow speed of 2 mm/s. CD4 roll over endothelial cells held by selectin-ligand interactions with a rate of 10 μm/s. The relatively small differences in kinetics we observed here, might be enough to favor the binding of IL7-activated cells with integrins activated by inside-out pathways. On the contrary, stochastic contacts with the ECM might be too short-lived in non-activated cells for the first integrin to activate the outside-in pathway (Hynes, 1992, 2002).

With these measurements, we demonstrate that scAFS can be used to study the adhesion process of hundreds of cells in parallel in real time using well-controlled forces. Because the parameters that influence the acoustic force experienced by cells, i.e. size, shape and density, are very homogeneous in CD4 (see **online methods**) (Laurell et al., 2007; Petersson et al., 2007), we could calibrate a subset of cells and use the calibration parameters obtained for the whole population. Calibration of all cells individually would, however, increase the accuracy of the rupture force determination and may be required for cell types with more heterogeneity. Here, we have applied forces up to 500 pN to adherent CD4. Since the maximum output voltage that can be applied (42 Vpp) to the piezo element with our current system, we can estimate that forces as high as 1 nN can be reached for these cells. Such forces are high enough to rupture multiple integrin-fibronectin bonds as shown here, or other cell adhesion systems in the early steps of adhesion such as integrins with CAM, VCAM and MADCAM ligands (Ley et al., 2007) or T-cell receptors with peptide-MHC complexes (Liu et al., 2014). However 1 nN will not be enough force to detach completely spread-out cells from a surface.

We performed measurements at room temperature and only fibronectin was used to mimic the ECM, a simplification in order to demonstrate the potential of the scAFS method. *In vivo*, the blood vessel wall is composed of endothelium cells, which express integrin ligands or ECM induced while activated, and in future experiments endothelium cells could be grown inside the flow chamber at 37 °C, providing a more realistic model for the vessel wall. When endothelium cells spread out, they cannot be detached by the acoustic force. T-cells could be flushed in such a prepared flow chamber, allowing one to investigate the full complexity of these cell-cell interactions using scAFS.

CONCLUSION

scAFS is a novel method that can be used to obtain insight into the cell adhesion process, it is performed in a closed fluidics system, allowing precise control of parameters such as temperature, flow rate and gases dissolved in the medium, which allows keeping the sample sterile and the operator safe. Given the volume of the AFS chamber (5.4 μL) measurements can be performed on small biological sample volumes, obtained for example from patients or small animals. This approach should be instrumental in the measurement of T-cell adhesion alteration associated with pathologies in diagnosis development or in drug screening (Ley et al., 2016). Finally, the relative simplicity and compactness of the system allows straightforward integration in advanced fluorescence microscopes. Taken together, this illustrates that acoustic forces can be applied directly to cells in order to assess quantitatively their interactions with their environment, opening up a wide range of potential applications in research and the clinic.

ACKNOWLEDGMENTS

The authors thank Andrea Candelli for helpful discussions (LUMICKS B.V.) and Jenneke Klein Nuland for providing lab facilities needed for cell culture (ACTA, Amsterdam). This work is part of the research program of Future & Emerging Technologies (FET) (E.J.G.P. and G.J.L.W.), which is part of the EU Horizon 2020 program, and supported by the Institut Pasteur through its Transversal Research Program (PTR 424)

and equipment funding (Center for Innovation and Technical Research), and by the Pasteur-Weizmann Foundation.

AUTHOR CONTRIBUTIONS

D.K., F.O., N.A., T.R. acquired scAFS data; S.G. and T.R. have purified, grown and prepared the CD4; D.K., F.O., N.A., P.B. and T.R. have analyzed data; D.K., P.B., G.W., E.P. and T.R. wrote the manuscript. G.W., E.P., and T.R. supervised the project.

COMPETING FINANCIAL INTERESTS

D.K., G.J.L.W. and E.J.G.P. have filed a patent application (PCT/NL2014/050377) covering the acoustic force spectroscopy method. G.J.L.W. and E.J.G.P. are co-owners of LUMICKS B.V.

Methods

Blood sampling and cell preparation

Blood samples from healthy donors were provided by a blood center (Etablissement Français du Sang, Centre Necker-Cabanel, Paris). CD4 were separated by negative selection (RosetteSep Kit, StemCell) as described previously (Tamarit et al., 2013). CD4 were equilibrated for 18 hours in RPMI 1640 medium (Lonza) supplemented with Hepes (10 mM, Sigma-Aldrich), penicillin 50 U/mL, streptomycin 50 μg/mL (Sigma) and heat-inactivated fetal bovine serum (FBS 10%, Lonza, uncomplemented at 53 °C during 45 min, containing 50mg of proteins per mL from which 40 mg/mL of BSA) and placed in an incubator at 37 °C, 5% CO_2 in a humidified atmosphere. CD4 were activated with 2 nM of recombinant glycosylated human IL7 expressed from HEK cells (Abcys) at 37 °C, 5% CO_2 for 15 minutes prior to injection in the scAFS flow chamber at room temperature.

Experimental setup, cell imaging

The AFS chip itself consists of a flow chamber and a piezoelectric element (LUMICKS b.v., AFS module). The fluid chamber surface area was 54 mm^2, 12 mm^2 under each of the two piezos (**Figure S1**). The functionalization of the flow chamber was performed by injecting 30μL of bovine fibronectin solution (5 μg/mL diluted in PBS, Sigma-Aldrich) incubated for 30 min at room temperature as described previously (Boettiger, 2007). The chamber was saturated with 30 μL of RPMI medium completed with 1% FBS for 15 min then washed with 200μL of the same medium (40 volumes of the chamber). For assessment of CD4 adhesion, 30 μL of non-activated or IL7-activated CD4 suspensions in RPMI medium, completed with Hepes (10 mM final) and 1% FBS (0.5 mg of proteins /mL final), was injected in the chamber and incubated at room temperature. The piezoelectric element attached to the flow chamber was driven with a function generator (Siglent, SDG830) providing oscillating current amplified by a RF-amplifier (SCD, ARS 2_30_30, 50 Ω impedance, 10 W maximum output power). A maximum driving voltage of 42 V_{pp} was applied in these experiments at 14.3 MHz for not more than a few seconds, this did not lead to sample heating of more than two degrees. Part of the data was acquired using a LUMICKS AFS Stand-alone instrument. Images were acquired with a bright field inverted microscope (Nikon Eclipse Ti). Here, an LED light source (Thorlabs, M660L4) was used in combination with an air objective lens (Nikon, CFI Plan Fluor 10X/0.30 NA, field of view 1.8 mm^2). To regulate the sample *z*-position, a piezo translation stage (PI, P-517.2CL) was mounted on the microscope and driven by a digital piezo-controller (PI, E-710.4CL). Images were taken with a CMOS camera (Thorlabs, DCC1545M, 1280x1024 pixels) with a full-frame rate of 60 Hz.

Cell tracking

Acquired images were processed in real time to extract the cell positions in three dimensions. To determine the *xy*-positions, a quadrant interpolation algorithm was used (van Loenhout et al., 2012). A look-up table (LUT) was used to determine the *z*-position (Gosse and Croquette, 2002). The LUT was built from image series of cells seating on the glass surface in the absence of acoustic force for cell individually. Images of seated cells were acquired starting from the cells completely in focus up to 30 µm above the focus, with 100 nm steps. The diffraction rings of CD4 were used to interpolate the *xyz*-positions of the cell centers. The precision of the tracking was determined by calculating the standard deviation of a bound cell during 8 seconds at 60 Hz, resulting in an accuracy of 2.0 nm *x* and *y*, and 72 nm in *z* (**Figure S2**). The tracking software is available at http://figshare.com/articles/AFS_software/1195874. For the real-time tracking of 300 cells in parallel, a fast PC (including two Xeon E5 2643v2 processors) running National Instruments LabView is used. Additionally, a moving ROI was implemented to adjust all the ROIs, frame-to-frame, bases to the previously determined *xy*-position. Separate calibration of cells takes only a few minutes, including data processing.

Validation of the integrin-fibronectin bonds

The specificity of the CD4 adhesion to fibronectin-functionalized glass through integrins has been validated using competitive peptide inhibitors: Arg-Gly-Asp and Gly-Arg-Gly-Asp-Ser (Sigma-Aldrich) (Bernhagen et al., 2017). Peptide solutions were added to non-activated or IL7-activated $CD4^+$ T-cell suspensions in RPMI medium completed with 1% fetal bovine serum (containing 40mg/mL of BSA, 0.4mg/mL final) and 50mM Hepes. Peptide/cell solutions of 10^{-7}, 10^{-6}, 10^{-5}, 10^{-4}, 10^{-3} o**r** 10^{-2} M of RGD or GRGDS were prepared. Peptide/cell samples were injected in the chamber and incubated at room temperature. Measurements have been performed in duplicate using CD4 isolated from three blood donors.

Acoustic force calibration on cells

The acoustic radiation force F_{rad} has been calibrated using the method previously described by Kamsma et al. (Kamsma et al., 2016) . Here the acoustic force was determined by writing down the force balance during the uplift of unbound cells. Acceleration was neglected, because the measurements were performed in the low Reynolds number regime:

$$F_{rad} - F_{gravity} + F_{buoyancy} - F_{drag} = 0 \qquad \textbf{(1)}$$

$F_{gravity}$, $F_{buoyancy}$ *and* F_{drag} are the gravitation, buoyancy and drag forces, respectively. The radiation force resulted from the calculation of the other forces:

$$F_{gravity} = 4/3\ \pi\ r^3\ \rho_{cell}\ g \qquad \textbf{(2)}$$
$$F_{buoyancy} = 4/3\ \pi\ r^3\ \rho_{medium}\ g \qquad \textbf{(3)}$$
$$F_{drag} = v_{cell}\ \gamma_{faxen} \qquad \textbf{(4)}$$

The CD4 are nearly perfect spheres with a radius r_{cell} of 4.01 ± 0.13 µm (n = 463). Radii were computed from optical microscopy from the 2D projection surface area of individual cell using ImageJ assuming perfect spheres. The density ρ_{cell} of CD4 is 1030 ± 20 kg·m^{-3}, determined from isopycnic sedimentation. The gravitational acceleration g is 9.81 m·s^{-2}. The density of medium ρ_{medium} (RPMI/10% FBS) is 1008.4 kg·m^{-3}, as determined using a gauged flask at 23 °C. Faxen's drag coefficient γ_{faxen}(Schaffer et al., 2007) was used to determine the drag force on the cells; this takes into account the hydrodynamic surface effect. The dynamic viscosity η_{medium} of the medium is 0.999 ± 0.007 mPa·s, as measured with an Ostwald's u-tube viscosimeter at 23 °C. The velocity of the cell v_{cell} was calculated by taking the derivative of the cell *z*-position versus time.

The cell sedimentation velocity, after acoustic elevation, was measured to verify the parameters used. Cells had a constant velocity of sedimentation for about 10 seconds, until they slowed down in close proximity of the glass surface due to the increase of the viscosity, as described by Faxen's law (Schaffer et al., 2007). The sedimentation apparent velocity of cells in the absence of acoustic pressure is given by:

$$v_{sedimentation} = 4/3\pi\, r^3 g\, (\rho_{cell} - \rho_{medium}) / (6\pi\eta\, r) = 2\, (\rho_{cell} - \rho_{medium})\, r_{cell}^{\,2}\, g / (9\, \eta) \qquad \textbf{(5)}$$

The sedimentation velocities of the individual CD4 were measured till the cell was reaching one diameter above the glass surface (8 μm), resulting $v_{sedimentation}$ = 1094 ± 33 nm·s^{-1} (n =10, **Figure 2G**). Considering that r_{cell} = 4.0 μm, it follows that the CD4 have a ρ_{cell} = 1038.7 ± 0.9 kg·m^{-3} at 23 °C.

The force on the CD4 was calibrated using **Expression 1**. The elevation velocity of the cells was used to determine the force for each time step (**Figure S4A,B**). A sine function (the theoretical shape of the force field) was fitted to the force versus cell height plot (**Figure S4C**). The force F_{rad} was then extrapolated for the cells seated on the bottom surface. The curve fitting was repeated for several acquisitions on multiple cells (n = 14 and 37 for non-activated and IL7-activated cells, respectively) with increasing voltage from 2.1 to 10.5 V_{pp}. The extrapolated forces F_{rad} versus voltage were plotted in order to verify the quadratic dependence of the force with the amplitude.

In order to quantify the homogeneity of the acoustic field of view, the force per square voltage of ~1500 silica microspheres (6.84 μm in diameter) are calibrated with the same method as described above. The calibration results in a ~30 % standard deviation of the acoustic force over the whole field of view (**Figure S4D**), this includes the error due to variations in microsphere size (~5% in radius, which will result in ~15% variation in applied force).

Investigating the strength of glass-adsorbed fibronectin

We test if cell detachment is caused by breaking of the cell-fibronectin bonds and not by breaking of the interaction of fibronectin with the glass surface. The glass surface inside the AFS chamber was functionalized with fibronectin (10 μg/mL in PBS, 30 min, room temperature) then washed with PBS. Carboxylic acid groups from glass-adsorbed fibronectin were activated by adding a solution of EDC (N-3-dimethylaminopropyl-N'-ethylcarbodiimide, 15 μL, 2 mM, Sigma-Aldrich) and NHS (N-hydroxy-succinimide, 15 μL, 5 mM, Sigma-Aldrich) diluted in PBS and incubated for 15 min at room temperature. Polystyrene microspheres functionalized with amine groups (2-aminoethylated beads, 5 μm in diameter, Sigma-Aldrich) were suspended in PBS and then injected in the chamber and incubated for 2 hours. Unbound microspheres were washed away with 200 μL of PBS. Forces were calibrated as described above, but using free microspheres in the absence of fibronectin (r_{bead} = 2.5 μm, ρ_{bead} = 1500 kg/m^3).

Determination of rupture forces

To measure the rupture force of a bound cell, a square-root amplitude ramp was applied, while the cell height is measured**.** The rupture force F_r was calculated by determining the voltage at rupture. Using the force/(voltage)^2 ratio, the rupture force is given by:

$$F_r = 0.554\ 10^{-12}\ U_r^2(t_r) \qquad \textbf{(7)}$$

During the force ramp, some cells showed small deformations before rupture, as shown in **Figure S5E**. These deformations affected the determination of the cell's *z*-position and exact determination of the rupture event was less evident. We considered a rupture event when the elevation of the cell was larger

than one diameter of the cell (8 μm). This definition resulted in a time delay between the "real" rupture event time t_r and the "considered" rupture time t_8 (when reaching 8 μm above the glass bottom surface, at amplitude U_8) (**Figure S5B)**. The real rupture time as a function of the t_8 and the amplitude U_8, is given by:

$$t_r = t_8 - (0.0386\, e^{-(0.372\, U_8)}) \qquad \textbf{(8)}$$

The time delay ($t_8 - t_r$) is shown in (**Figure S5B**), where the amplitude U_r driving the rupture of the CD4 from the fibronectin-functionalized surface is given by:

$$U_r = U_8 \sqrt{\left(\frac{(t_8 - t_r)}{t_{max}}\right)} \qquad \textbf{(9)}$$

As shown in **Figure S5F,** cells were first subjected to a series of nine acoustic pulses (14.3 MHz, 4.2 V_{pp}, 2 s) spaced by 2 minutes (blue line) to determine whether they were unbound, binding or bound cells. Subsequently, in order to determine the cells' adhesion strength, a square root amplitude ramp (14.3 MHz, 0-42 V_{pp}, 18 s) was applied after 19 min providing a linear force ramp (0 – 970 pN, 53.88 pN/s).

References

Benoit, M., Gabriel, D., Gerisch, G., and Gaub, H.E. (2000). Discrete interactions in cell adhesion measured by single-molecule force spectroscopy. Nat Cell Biol *2*, 313-317.

Bernhagen, D., De Laporte, L., and Timmerman, P. (2017). High-Affinity RGD-Knottin Peptide as a New Tool for Rapid Evaluation of the Binding Strength of Unlabeled RGD-Peptides to alphavbeta3, alphavbeta5, and alpha5beta1 Integrin Receptors. Anal Chem *89*, 5991-5997.

Boettiger, D. (2007). Quantitative measurements of integrin-mediated adhesion to extracellular matrix. Methods Enzymol *426*, 1-25.

Butcher, E.C. (1991). Leukocyte-endothelial cell recognition: three (or more) steps to specificity and diversity. Cell *67*, 1033-1036.

Cimbro, R., Vassena, L., Arthos, J., Cicala, C., Kehrl, J.H., Park, C., Sereti, I., Lederman, M.M., Fauci, A.S., and Lusso, P. (2012). IL-7 induces expression and activation of integrin alpha4beta7 promoting naive T-cell homing to the intestinal mucosa. Blood *120*, 2610-2619.

Dustin, M.L., and Springer, T.A. (1989). T-cell receptor cross-linking transiently stimulates adhesiveness through LFA-1. Nature *341*, 619-624.

Friedland, J.C., Lee, M.H., and Boettiger, D. (2009). Mechanically activated integrin switch controls alpha5beta1 function. Science *323*, 642-644.

Garcia, A.J., Huber, F., and Boettiger, D. (1998). Force required to break alpha5beta1 integrin-fibronectin bonds in intact adherent cells is sensitive to integrin activation state. J Biol Chem *273*, 10988-10993.

Gosse, C., and Croquette, V. (2002). Magnetic tweezers: micromanipulation and force measurement at the molecular level. Biophys J *82*, 3314-3329.

Hogan, B., Babataheri, A., Hwang, Y., Barakat, A.I., and Husson, J. (2015). Characterizing cell adhesion by using micropipette aspiration. Biophys J *109*, 209-219.

Hynes, R.O. (1992). Integrins: versatility, modulation, and signaling in cell adhesion. Cell *69*, 11-25.

Hynes, R.O. (2002). Integrins: bidirectional, allosteric signaling machines. Cell *110*, 673-687.

Kamsma, D., Creyghton, R., Sitters, G., Wuite, G.J., and Peterman, E.J. (2016). Tuning the Music: Acoustic Force Spectroscopy (AFS) 2.0. Methods *105*, 26-33.

Kim, S.H., Chegal, W., Doh, J., Cho, H.M., and Moon, D.W. (2011). Study of cell-matrix adhesion dynamics using surface plasmon resonance imaging ellipsometry. Biophys J *100*, 1819-1828.

Kinashi, T. (2012). Overview of integrin signaling in the immune system. Methods Mol Biol *757*, 261-278.

Kondrack, R.M., Harbertson, J., Tan, J.T., McBreen, M.E., Surh, C.D., and Bradley, L.M. (2003). Interleukin 7 regulates the survival and generation of memory CD4 cells. J Exp Med *198*, 1797-1806.

Laurell, T., Petersson, F., and Nilsson, A. (2007). Chip integrated strategies for acoustic separation and manipulation of cells and particles. Chem Soc Rev *36*, 492-506.

Lehenkari, P.P., and Horton, M.A. (1999). Single integrin molecule adhesion forces in intact cells measured by atomic force microscopy. Biochem Biophys Res Commun *259*, 645-650.

Ley, K., Laudanna, C., Cybulsky, M.I., and Nourshargh, S. (2007). Getting to the site of inflammation: the leukocyte adhesion cascade updated. Nat Rev Immunol *7*, 678-689.

Ley, K., Rivera-Nieves, J., Sandborn, W.J., and Shattil, S. (2016). Integrin-based therapeutics: biological basis, clinical use and new drugs. Nat Rev Drug Discov *15*, 173-183.

Li, F., Redick, S.D., Erickson, H.P., and Moy, V.T. (2003). Force measurements of the alpha5beta1 integrin-fibronectin interaction. Biophys J *84*, 1252-1262.

Liu, B., Chen, W., Evavold, B.D., and Zhu, C. (2014). Accumulation of dynamic catch bonds between TCR and agonist peptide-MHC triggers T cell signaling. Cell *157*, 357-368.

Lu, H., Koo, L.Y., Wang, W.M., Lauffenburger, D.A., Griffith, L.G., and Jensen, K.F. (2004). Microfluidic shear devices for quantitative analysis of cell adhesion. Anal Chem *76*, 5257-5264.

Marx, V. (2015). Biophysics: using sound to move cells. Nat Methods *12*, 41-44.

Mazzucchelli, R., and Durum, S.K. (2007). Interleukin-7 receptor expression: intelligent design. Nat Rev Immunol *7*, 144-154.

Petersson, F., Aberg, L., Sward-Nilsson, A.M., and Laurell, T. (2007). Free flow acoustophoresis: microfluidic-based mode of particle and cell separation. Anal Chem *79*, 5117-5123.

Reyes, C.D., and Garcia, A.J. (2003). A centrifugation cell adhesion assay for high-throughput screening of biomaterial surfaces. J Biomed Mater Res A *67*, 328-333.

Schaffer, E., Norrelykke, S.F., and Howard, J. (2007). Surface forces and drag coefficients of microspheres near a plane surface measured with optical tweezers. Langmuir *23*, 3654-3665.

Schnoor, M., Alcaide, P., Voisin, M.B., and van Buul, J.D. (2015). Crossing the Vascular Wall: Common and Unique Mechanisms Exploited by Different Leukocyte Subsets during Extravasation. Mediators Inflamm *2015*, 946509.

Settnes, M., and Bruus, H. (2012). Forces acting on a small particle in an acoustical field in a viscous fluid. Phys Rev E Stat Nonlin Soft Matter Phys *85*, 016327.

Sitters, G., Kamsma, D., Thalhammer, G., Ritsch-Marte, M., Peterman, E.J., and Wuite, G.J. (2015). Acoustic force spectroscopy. Nat Methods *12*, 47-50.

Spengler, J.F., Coakley, W. T. & Christensen, K. T. (2003). Microstreaming effects on particle concentration in an ultrasonic standing wave. AIChE J *49*, 2773–2782.

Springer, T.A. (1994). Traffic signals for lymphocyte recirculation and leukocyte emigration: the multistep paradigm. Cell *76*, 301-314.

Tamarit, B., Bugault, F., Pillet, A.H., Lavergne, V., Bochet, P., Garin, N., Schwarz, U., Theze, J., and Rose, T. (2013). Membrane microdomains and cytoskeleton organization shape and regulate the IL-7 receptor signalosome in human CD4 T-cells. J Biol Chem *288*, 8691-8701.

van Loenhout, M.T., Kerssemakers, J.W., De Vlaminck, I., and Dekker, C. (2012). Non-bias-limited tracking of spherical particles, enabling nanometer resolution at low magnification. Biophys J *102*, 2362-2371.

FIGURE LEGENDS

Figure 1: CD4-adhesion mechanism

Three-step mechanism of leukocytes adhering to blood-vessel endothelium while infiltrating inflamed or infected tissues (Butcher, 1991; Ley et al., 2007; Schnoor et al., 2015; Springer, 1994). ***Step 1***: unbound CD4 (pink) carried by the blood flow in end-vessels, rolling along the vascular endothelium (brown rectangles), while P-selectin glycoprotein ligand-1 at the CD4 surface bind transiently to endothelial cell adhesion molecules, first to L-selectins (brown sticks), later, upon inflammation to P-selectins (green sticks). ***Step 2***: chemokines or cytokines (black diamonds) expressed or presented by inflamed endothelial cells, bind their cognate receptors at the surface of CD4 and trigger intracellular signals that activate different kinds of integrin dimers $\alpha\beta$ (pink lollipops) targeting the ECM ($\alpha4\beta1$, $\alpha5\beta1$ and $\alpha6\beta1$) and ligands such as ICAM ($\alpha L\beta2$), VCAM ($\alpha4\beta1$) and MADCAM ($\alpha4\beta7$) (brown baskets) (Ley et al., 2007). CD4 slow down and crawl along the surface. ***Step 3***: CD4 are immobilized by the formation of multiple integrin-ligand bonds. Subsequently, the CD4 cross the endothelium, and infiltrate the tissue.

Figure 2: scAFS on single CD4: manipulation and high-resolution tracking.

(**A**) Sketch showing CD4 (pink) in culture medium (light pink) in the AFS flow chamber, and sedimented on glass (blue) functionalized with fibronectin (FN, orange). (**B**) Digital image of CD4 on FN-functionalized glass in AFS flow chamber. (**C**) A standing acoustic wave induces a pressure force field (gray gradient) pushing the unbound cells (blue square) upward (dark, high pressure) to the acoustic node (light pink, low pressure). (**D**) Same cropped frame as in panel **B**, after the application of an acoustic wave (14.3 MHz, 4.2 V_{pp}, 5 s). Bound cells are immobile (orange square, the diffraction pattern is unchanged) and unbound cells have moved up towards the acoustic node, out of focus (blue square, the diffraction pattern has changed). For full fields of view see **Figure S1E-H**. Image series of a bound and an unbound cell, demonstrating the diffraction pattern of the cells upon application of acoustic force (**F** and **G)** *xy*- and *z*-position graphs as a function of time of unbound (blue) and bound (orange) CD4. Gray zones indicate the period of application of acoustic waves; black plots the amplitude of the acoustic wave (14.3MHz, 4.2Vpp, 5s). The center positions of CD4 at bottom surface and acoustic node are indicated by horizontal dashed black lines.

Figure 3: Deciphering unbound, binding and bound cells from their *xy*-trajectories and *z*-elevation.

Trajectories of CD4 *z*- (**left**) and *xy*-positions (**right**) have been plotted for representative cells from free (**A**), binding (**B**) and bound (**C**) subsets. CD4 are subjected to a series of nine acoustic pulses (14.3 MHz, 4.2 V_{pp}, 2 s), spaced by ~2 minutes as indicated in the plot (**A**, left). Color coding of the trajectories is used to indicate time correspondence between left and right plots. Purple and orange zones indicate whether cells are in the binding (adhesion process) or bound (immobilization) state, respectively.

Figure 4: CD4 adhere faster to fibronectin and get immobilized when activated by IL7.

(A, B) CD4 are activated by IL7 (+IL7, n = 666) or not (NA, n = 463) and subsequently injected in non-functionalized (-FN) or fibronectin-functionalized (+FN) chambers. The non-activated (NA, green) and IL7-activated cells (+IL7, red) are pushed upwards with a minimal force (14.3 MHz, 4.2 V_{pp}, 2 s) after 5, 20, 40 and 60 minutes of incubation. (**A**) Images of CD4 before (red) and after (green) acoustic wave application are superimposed (20 minutes of incubation). Immobile cells appear in yellow (superposition of red + green). Bound fractions (*xy*-shift < 1μm) are indicated. Bottom images show zooms of regions indicated by squares in top images. (**B**) Box plot of shifts in *xy*-plane of non-activated (green) and IL7-activated (red)

cells after 20 min of incubation in chambers functionalized with fibronectin (+FN) and not (-FN). For other time points see **Figure S3.** Whiskers are maximum and minimum, boxes indicate second and third quartiles framing the median. Bound fractions (*xy*-shift < 1mm, dashed orange threshold) are indicated on top of each column. (**C**) Cumulative probability distribution plot of the cell *xy*-shift, determined before and after acoustic force application, measured subsequently at 5, 20, 40 and 60 minutes incubation. Bound (orange), binding (purple) and unbound (blue) zone have a *xy*-shift of < 1, 1-3 and > 3 μm, respectively. (**D**) Adhesion of CD4 to the fibronectin-functionalized glass, challenged with increasing concentrations of peptide inhibitor Arg-Gly-Asp (RGD; plain line) and Gly-Arg-Gly-Asp-Ser (GRGDS; dashed line), after 20 minutes at 23 °C. This experiment has been performed on three different blood donors (error bars are s.e.m.). (**E**) Fraction cells bound as a function of time, plotted for non-activated and IL7-activated CD4 on glass functionalized or not with fibronectin.

Figure 5: CD4 rupture-force calibration and measurement.

(**A**) *z*-position of a representative unbound CD4 plotted with the voltage of the applied acoustic pulses (2.1, 4.2, 6.3, 8.4, 10.5 V_{pp}, <2 seconds). (**B**) Acoustic-pressure induced upward motion of the cell in panel **A.** Trajectories of different acoustic pulses are superimposed by adjusting time offset. Acoustic pulse is indicated by grey zone. The inset shows trajectories at a different time scale (from 0 to 30 seconds), focusing on sedimentation of cells after application of acoustic pulse (grey vertical line). (**C**) Force acting on the cell close to the bottom surface, as calibrated from the velocity in panel **B,** for cells from a representative donor (data are means ± s.d., n = 14 for not-activated and n = 37 for IL7-activated cells). Quadratic fits yield quadratic constants of 0.55 ± 0.25 and 0.54 ± 0.32 pN/V_{pp}^2 (fit value ± s.d.) for non-activated and IL7-activated cells, respectively. (**D**) Application of a linear (V_{pp}) ramp to a cell to determine rupture force (blue, 14.3 MHz, 0 to 10.5 V_{pp}). Corresponding complete field of view: see **Figure S1E-H** and **Supplemental Movie**. Most bound cells experience small upward movements (up to 3 μm) before rupture occurs. t_0 (vertical blue dashed line) indicates the start of acoustic force application, t_r (vertical red dashed line) the time of rupture identified here by a displacement of a cell larger than its diameter (8 μm). Amplitude of acoustic wave is indicated at bottom (black line). (**E-I**) The resistance of glass-adsorbed fibronectin to traction has been performed using polystyrene microspheres (5 μm in diameter) covalently bound to the fibronectin-functionalized glass**.** An upward acoustic force is applied to the beads from 0 to 500 pN in 2 seconds. (**G**) A representative part of the field of view is shown, boxes indicate the beads selected for *xyz*-position tracking. Images before (**F**) and after (**G**) force application of the same region are superposed (**H**) and show no detectable lateral shifts of any beads (<200nm; red+green=yellow). (**I**) The *z*-position of a representative bead is plotted versus time. The force ramp is indicated by a gray zone. Maximal elevation is 150 nm from the starting position.

Figure 6: CD4 rupture-force distribution, effect of IL7.
(**A**) Rupture force distribution of the CD4 from the fibronectin-functionalized surface (for underlying data analyses see **Figure S5**). Whiskers are maximum and minimum, boxes indicate second and third quartiles framing the median. Medians for unbound, binding and bound are 8.8 (n = 127), 39.8 (n = 41), 99.7 (n = 51) pN for non-activated and 14.8 (n = 160), 39.3 (n = 74), 111.7 (n = 107) pN for IL7-activated cells. Data separated for two representative blood donors are shown in **Figure S6**. (**B**) Bar plots of fractions of unbound, binding and bound cells out of non-activated and activated CD4 after 19 minutes of incubation (error bars are s.e.m.). (**C**) Cumulative probability distribution plot of the rupture forces is shown for unbound, bonding, and bound cell, IL7-activated and non-activated. The horizontal black dashed line indicates 50% of the cell subset. The vertical black dashed line indicates the change of force scale in abscise from 0-55 pN to 55-500pN.

SUPLEMENTAL DATA

Supplemental movie:
As shown in Figure 5D, human primary $CD4^+$ T-cells are imaged (60 images/s) when they are subjected during 20 seconds to an acoustic force ramp from 0 to 10.5 V_{pp} corresponding to forces of 0-55 pN. Weakly bound cells are lifted off the fibronectin-functionalized glass.

Figure 1

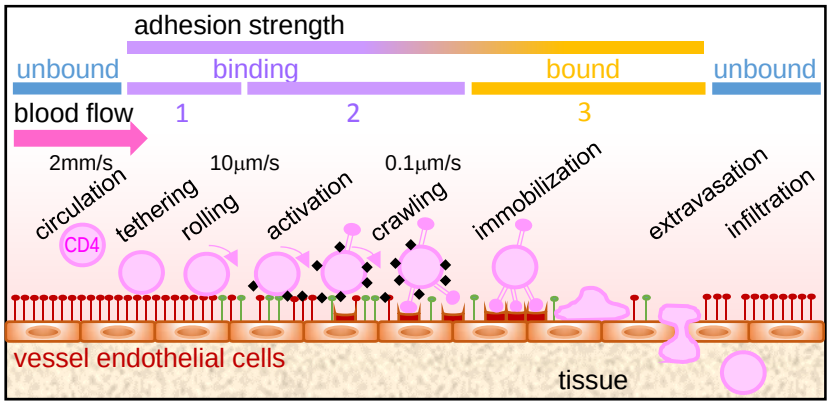

Figure 1

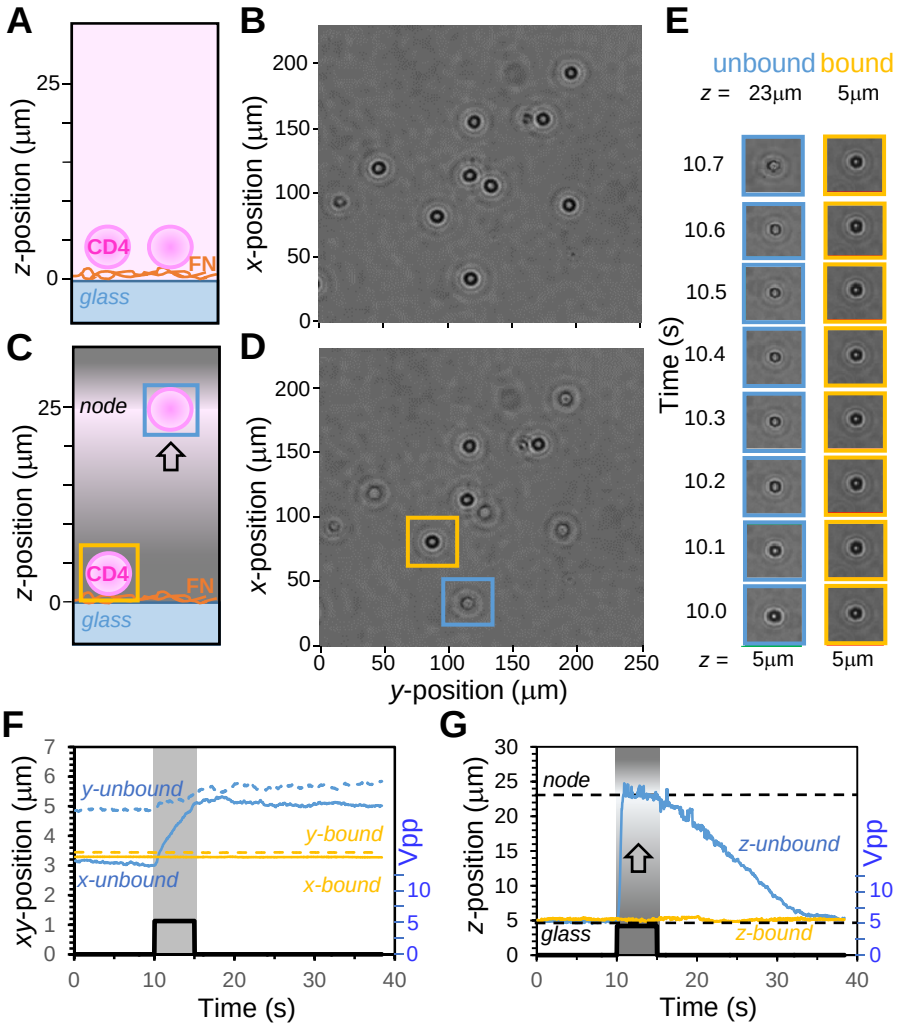
A
B
C
D
E
F
G
z-position (μm)
x-position (μm)
y-position (μm)
CD4
FN
glass
node
unbound
bound
z = 23μm
5μm
Time (s)
xy-position (μm)
Vpp
y-unbound
y-bound
x-unbound
x-bound
z-position (μm)
z-unbound
z-bound

Figure 2

Figure 3

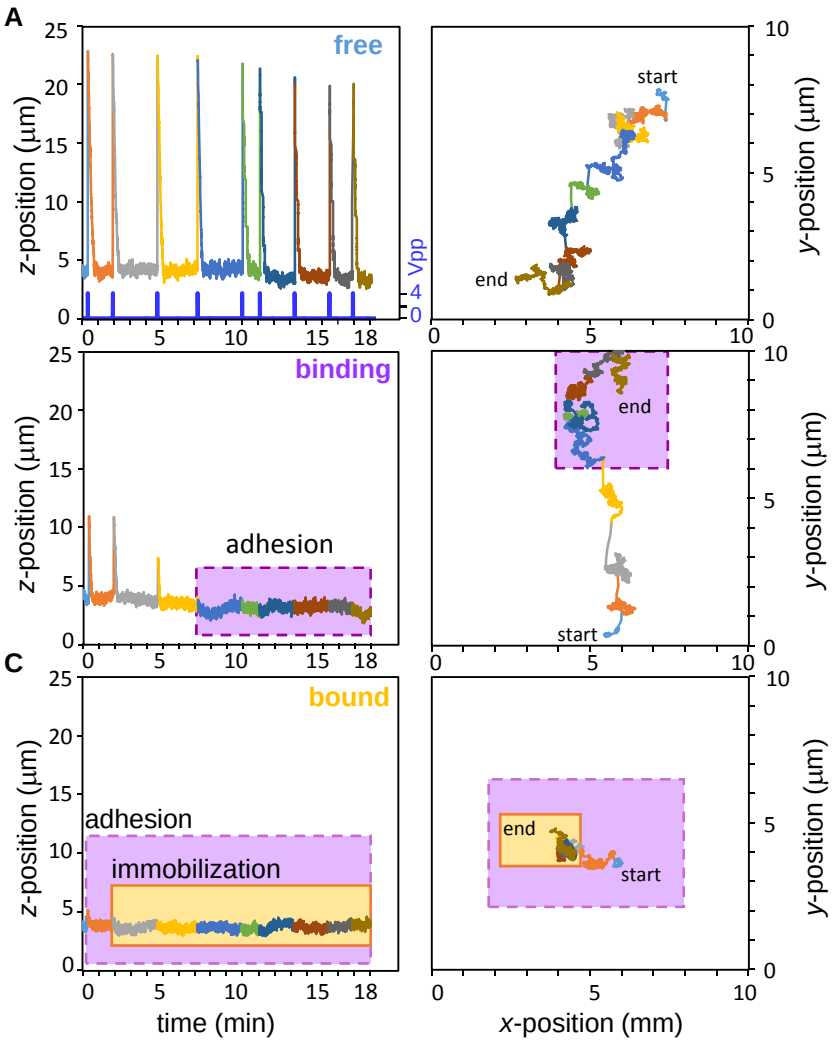

Figure 3

Figure 4

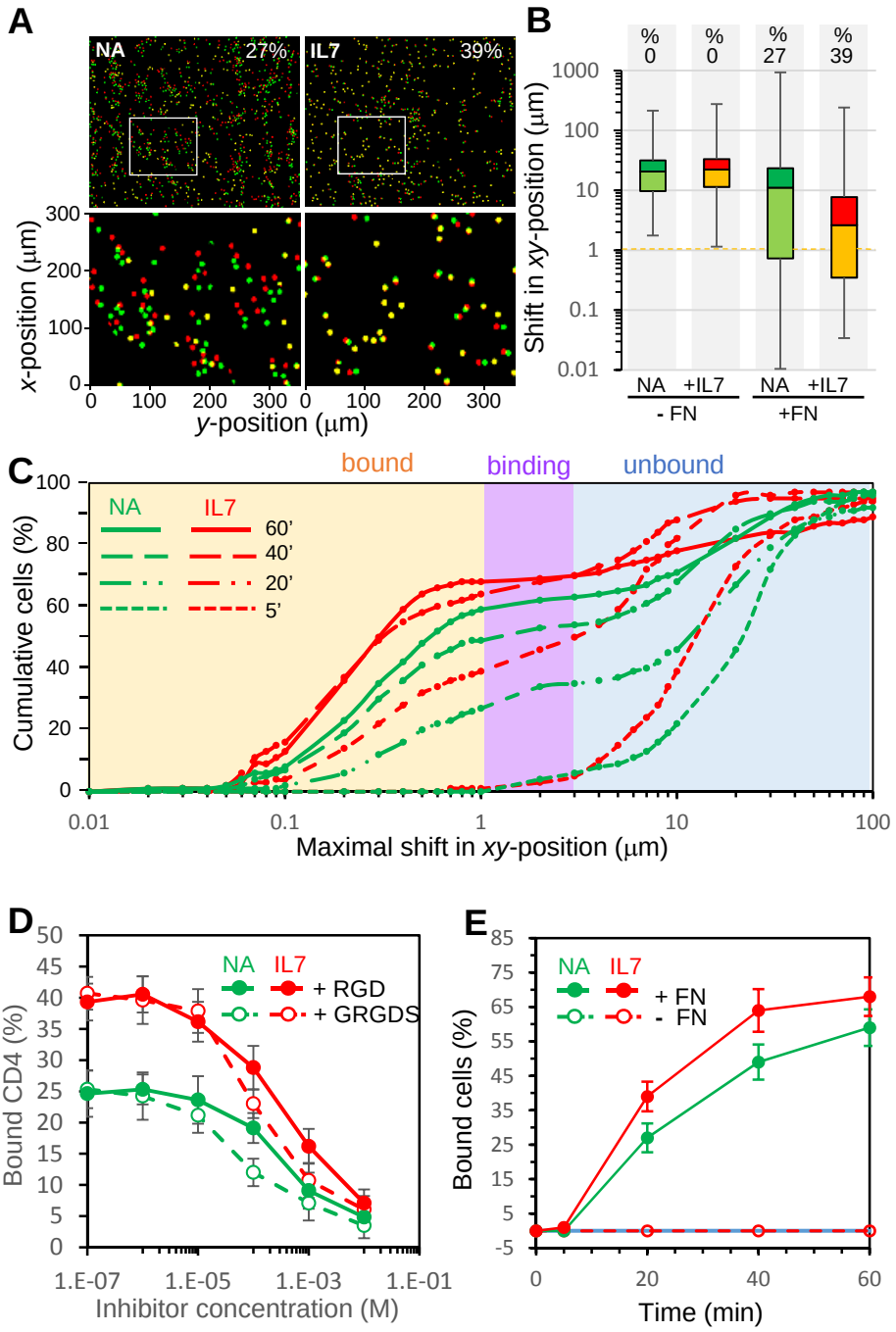

Figure 4

Figure 5

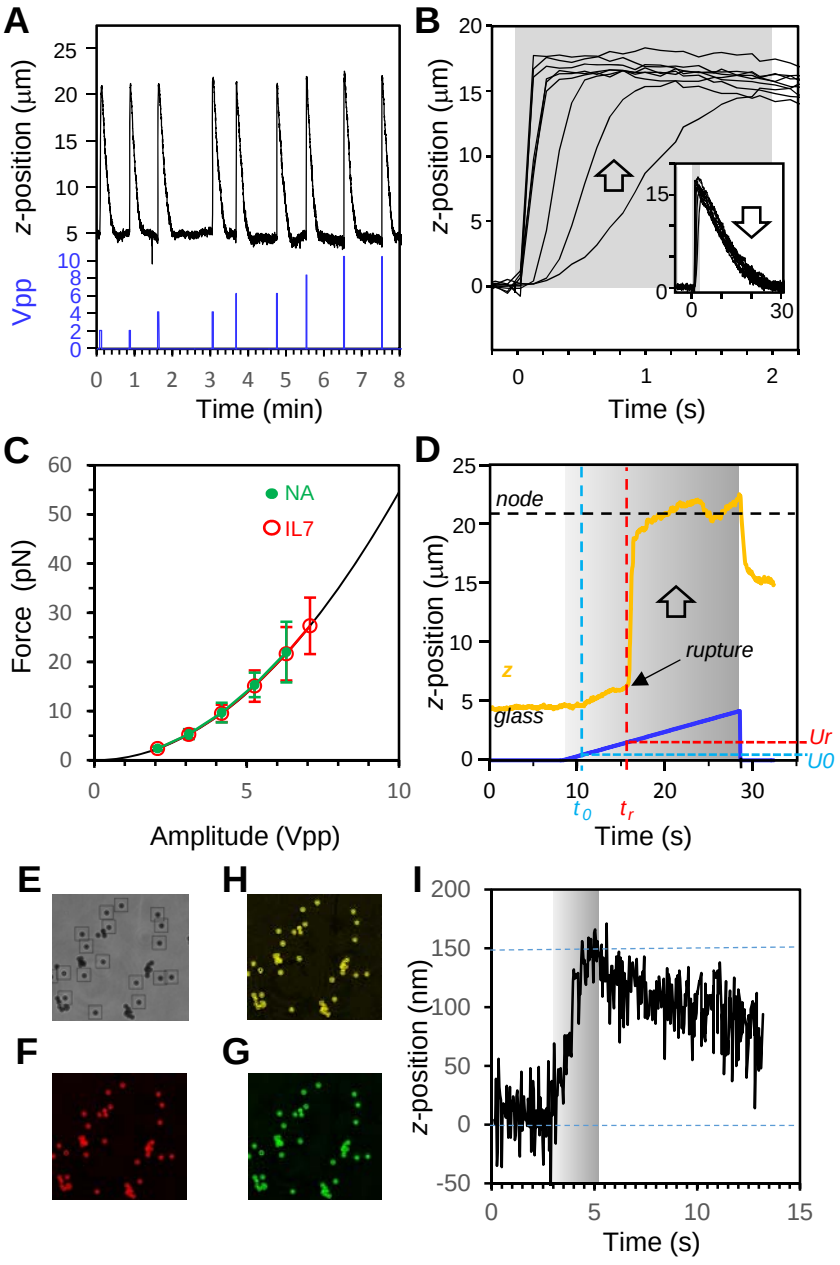

Figure 5

Figure 6

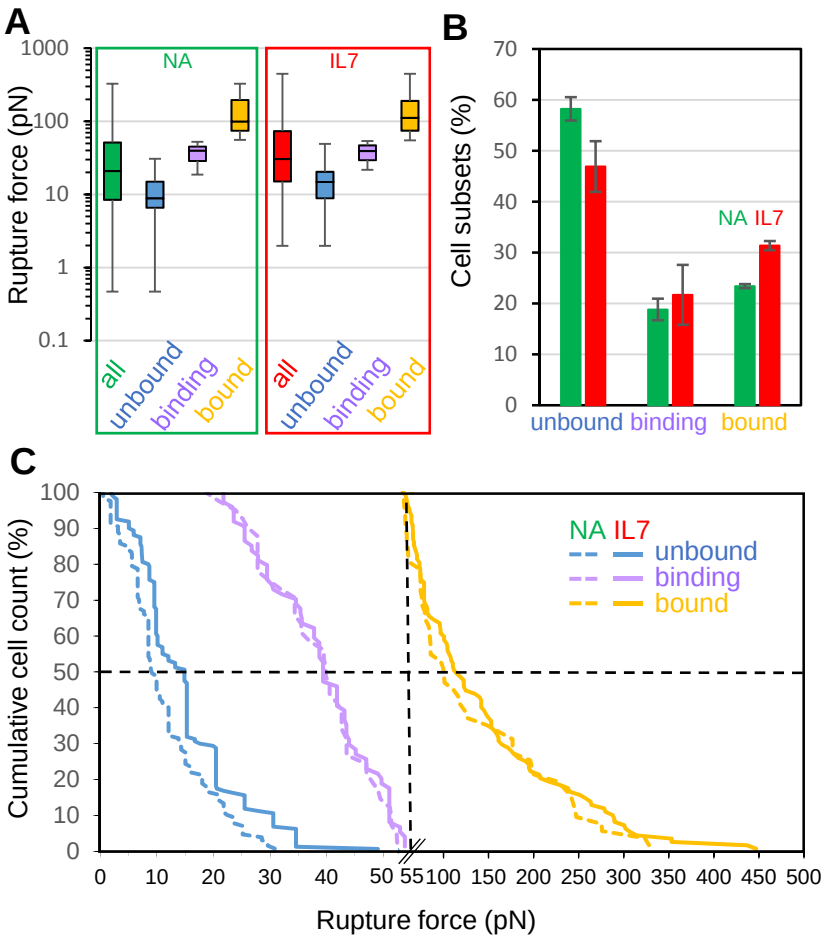

Figure 6

Figure S1: Description of the single-cell AFS system to assess cell-adhesion strength, related to Figure 2.

(**A**) As described in the experimental setup in Methods, the AFS chip consists of two glass plates (thickness 1 mm (top) and 0.17 mm (bottom)) with a fluid chamber (30 mm long, 1.8 mm wide, 0.1 mm thick, 5.4 mL volume, colored in pink) in between. Two independent transparent piezoelectric elements (7x7 mm) are glued to the upper glass slide. (**B**) Schematic illustration of the scAFS bright-field imaging method, using a LED, condenser lens, microscope objective and CMOS camera. The *z*-position of the AFS chip is controlled by a piezoelectric translation stage. (**C**) Schematic illustration of the transverse plane of the AFS chip (not to scale). An acoustic force gradient is shown (grey scale), with high force at the glass bottom plane and no force at the level of the acoustic node plane. Bound cells stay on the fibronectin, whereas unbound cells are pushed upward to the node. (**D**) A diagram of the hardware connected electronically to the piezo. A computer controls the function generator that feeds an alternating voltage via the amplifier to the piezoelectric element. (**E**) A digital camera acquires the images of CD4 in the field of view. (**F-I**) Images of field of views and zoom in showing CD4 injected in the FN-functionalized fluid chamber of the AFS chip (left) and schematic illustration (right). The objective is focused on the cells seated on the glass bottom surface; (**F**) no acoustic force is applied. (**G, H**) A linear acoustic amplitude ramp applies a quadratic force ramp to the cells (14.3 MHz, 0-10.5 Vpp, 20 s), lifting up first unbound cells (**G**, ~4.2 Vpp) and next binding cells (**H**, ~10.5 Vpp). Cells cluster together in lines, due to weak acoustic pressure deviations within the *xy*-plane (Spengler, 2003). (**I**) When the acoustic forces are off, all the cells sediment (~20 s), back to the focal plan. This data is also presented in Supplementary Movie.

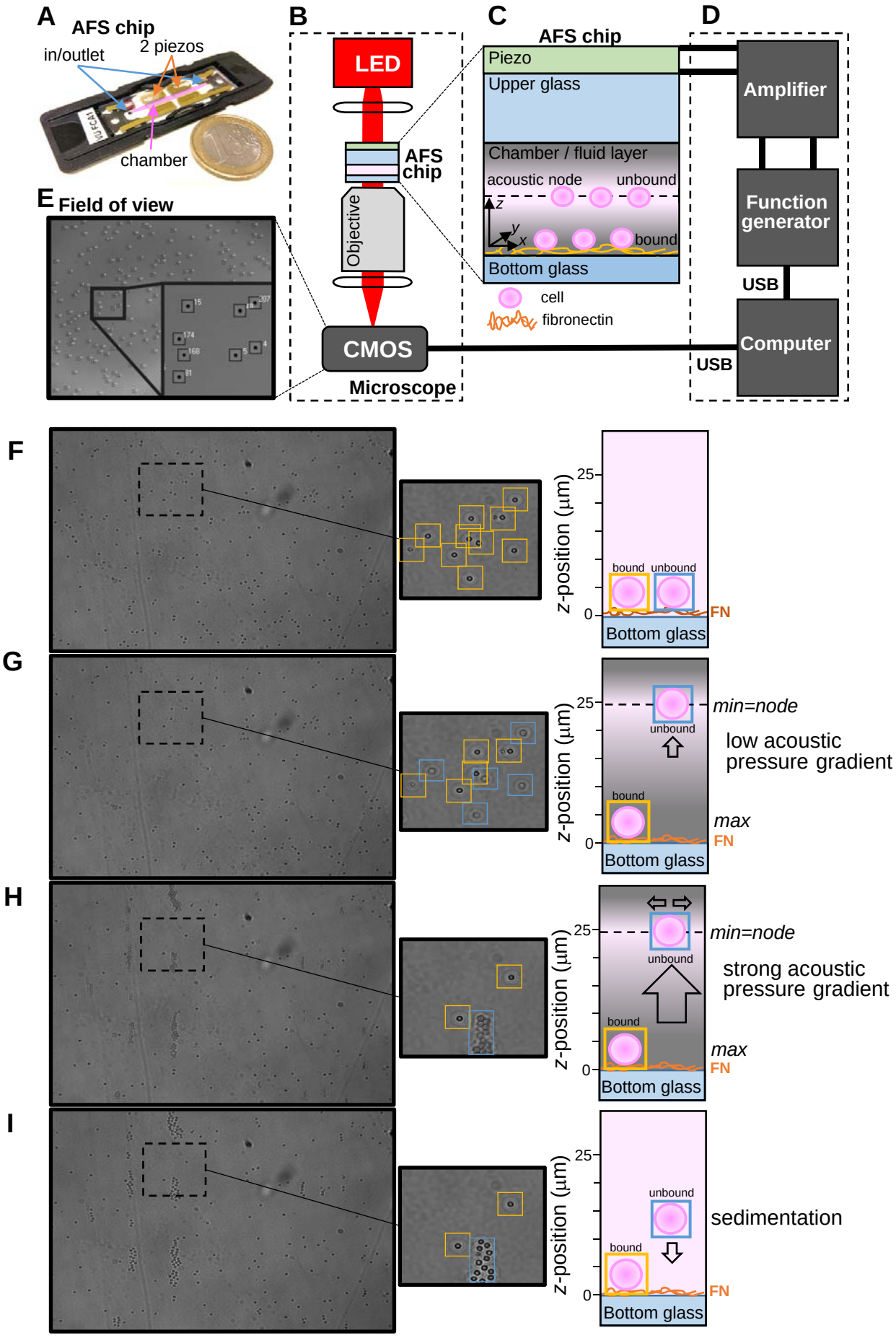

Figure S1: Description of the single-cell AFS system to assess cell-adhesion strength, related to Figure 2.

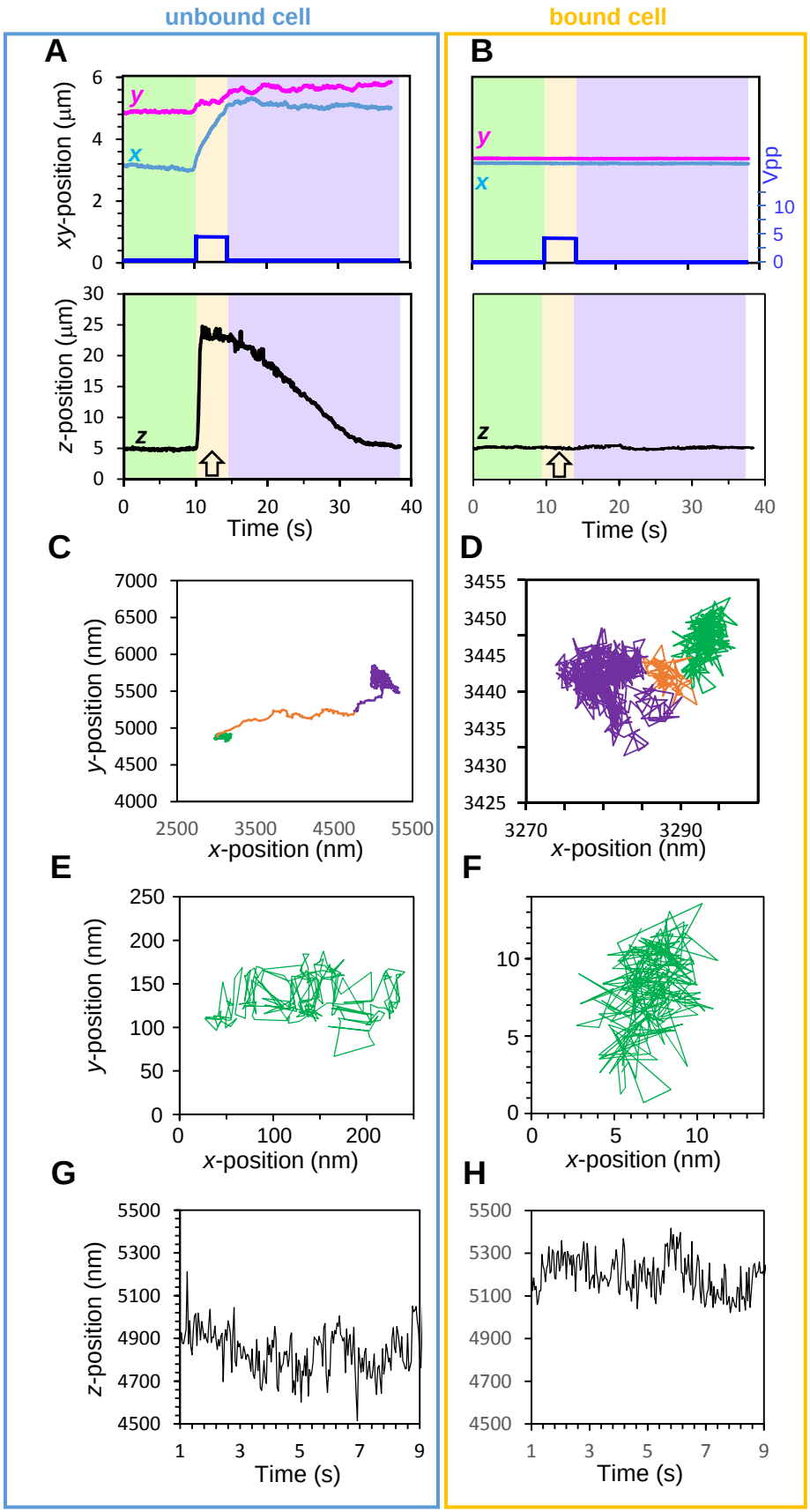

Figure S2: *x*, *y* and *z*-position tracking analysis and resolution, related to Figure 2.
(**A, B**) *xyz*-position trajectories of an unbound (left) CD4 and a bound (right) CD4. Same data as **Figure 2 F,G,** split in four panels. First, cells are seated on the surface of the flow cell (green zone); after 10 seconds, the acoustic force is applied (14.3 MHz, 4.2 V_{pp}, yellow zone); finally, the force is switched off (purple zone). (**C, D**) *xy* plot of the data shown in a and b, colors correspond to zones indicated in **A** and **B**. (**E, F**) *xy* plot of green zone, standard deviations are 36.3 and 1.6 nm for the unbound and bound CD4, respectively. (**G, H**) trajectories of *z*-position in the absence of force; standard deviations are 84 nm and 72 nm for the unbound and bound CD4, respectively.

Figure S3: CD4 adhesion kinetics to fibronectin assessed by scAFS, related to Figure 4.

(**A**) Supplement to **Figure 4A** showing the underlying data of **Figure 4C.** Non-activated and IL7-activated CD4 are injected in the FN-functionalized chamber at room temperature. CD4 are pushed upward with a minimal force (14.3 MHz, 4.2 V_{pp}, 2 s) to validate the fraction of unbound, binding and bound cells, after 5, 20, 40 and 60 minutes of incubation. Images of CD4 before (red) and after (green) acoustic wave application are shown superposed. Immobile cells appear in yellow (superposition green + red). Percentage of immobile cells (*xy*-shift < 1 mm) are indicated in white on the upper right corner. (**B**) Supplement to **Figure 4B** showing box plot of the *xy*-shifts after 5, 20, 40, 60 minutes of incubation for non-activated (green) and IL7-activated (red) CD4 on FN-functionalized glass. Whiskers are maximum and minimum values, and boxes indicate second and third quartiles framing the median. The horizontal blue bars indicate the average of *xy*-shifts amongst the cell subset with less than 1 mm of *xy*-shift (bound subset) and the percentage of these bound subsets are indicated above the corresponding columns.

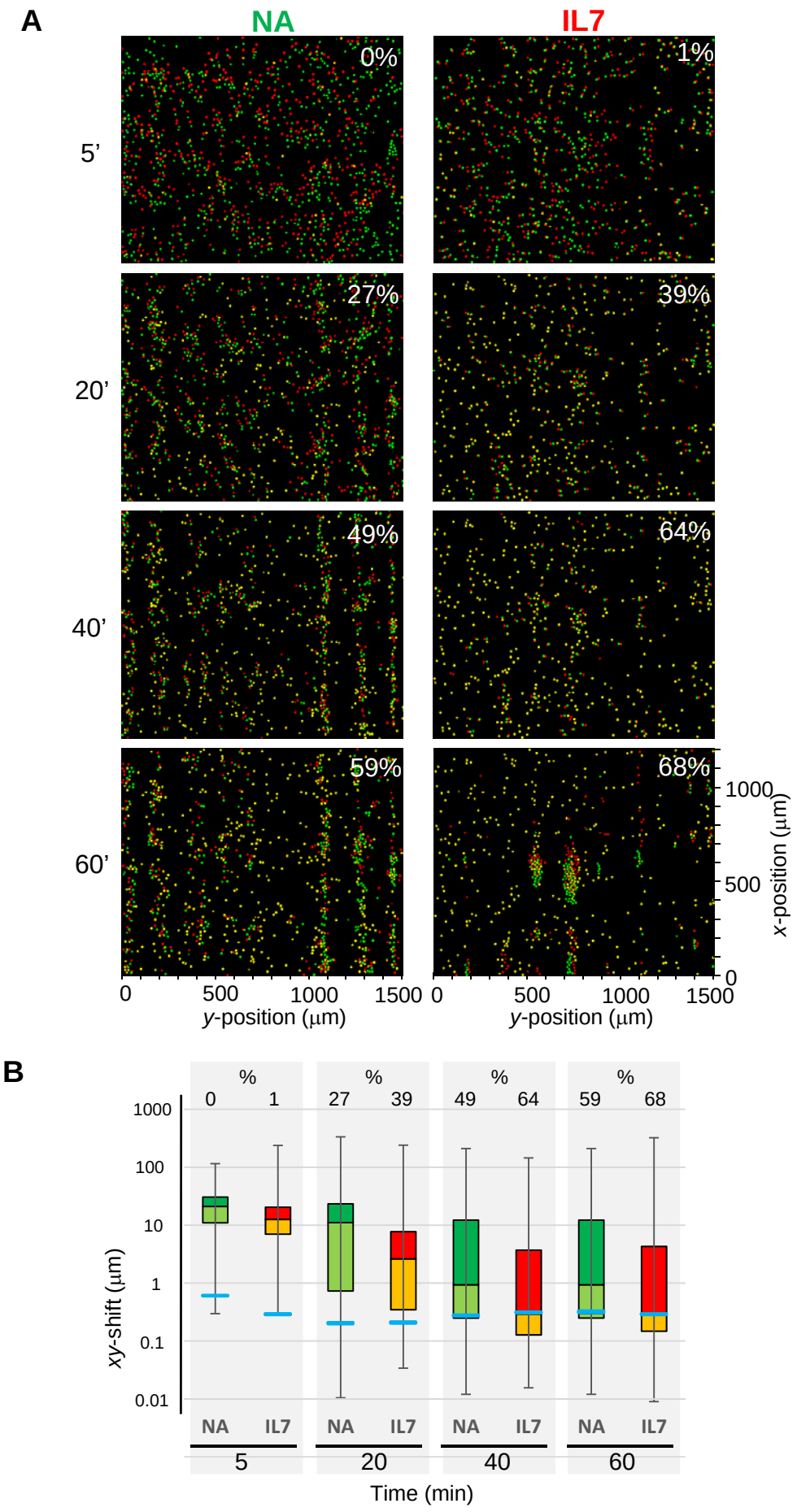

Figure S3: CD4 adhesion kinetics to fibronectin assessed by scAFS, related to Figure 4.

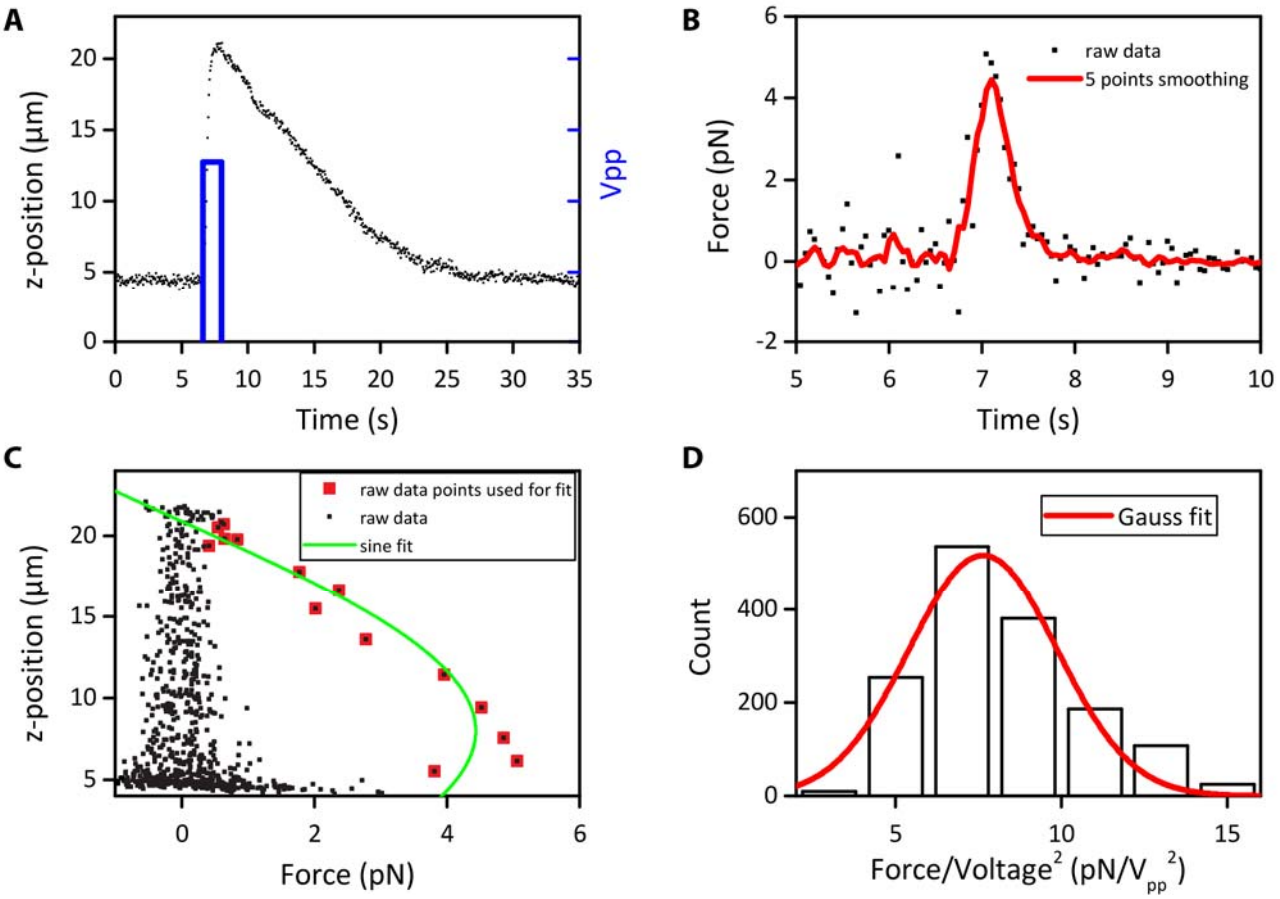

Figure S4: Force exerted by acoustic waves on the CD4 as a function of *z*-position, related to Figure 5.

(**A**) *z*-position trajectory of a single cell during application of sound wave (14.3 MHz, 4.2 V_{pp}, 2 s). (**B**) The acoustic radiation force F_{rad} is computed for every data point from the uplift velocity of the cell (v_{cell}), according to **Expression 12** of **Method** and plotted as a function time. Raw data (black dots) and moving average of 5 data points (red line) are displayed. (**C**) F_{rad} as a function of *z*-position with a sine function fitted to the data (green line). Red squares indicate the time points used for the fit from immediately after force application up to the moment the cell reaches the acoustic node. (**D**) The bar graph displays force / voltage^2 measured for silica microspheres (6.84 mm of diameter) over the over the full field of view (1.8 mm^2), as in panel **A**-**C**. Microspheres are suspended in PBS with and addition of 0.2 % w/v of BPS and 0.2 % w/v pluronics to prevent sticking to the surface. The histogram is fitted with a Gaussian function resulting in ~30 % standard deviation of the acoustic force, this includes the error due to the microsphere (~5% in radius, which will result in ~15% variation in applied force).

Figure S5: Determination of the exact rupture force of CD4, related to Figure 5.

(**A**) Force calibration was performed by applying increasing acoustic pulses (2.1, 4.2, 6.3, 8.4, 10.5 V_{pp} as indicated for each curve) for ~1 second to CD4 as shown in **Figure 5A,B**. Trajectories of the *z*-position of a representative cell are plotted. The horizontal green and red dash lines represent 0 and 8 mm elevation, respectively. The time t_0 is the moment of acoustic force application (vertical blue dashed line) and the time t_8 is the moment when the elevation of the cell is 8 mm higher (vertical red dashed line). (**B**) The time delay t_8-t_0 is plotted versus the amplitude U_8 and fitted with the **Expression 8** in **Methods**. The five data points obtained from panel **A** are plotted as open circles. Standard deviation of U_8 and time delay are indicated as error bars (n = 8). (**C**) The amplitude U_8 is plotted as a function of U_0 for non-activated and IL7-activated CD4 from two donors. The extrapolation of U_8 is plotted as a black line according to the **Expression 9** in **Methods**. Three of the data points from panel **A** are displayed as open circles, colors are used for the different subsets of cells (not-activated and IL7-activated cells of two different donors). The interpretation of the contributions of cell deformation and bond rupture to the *z* elevation are indicated as dashed arrows as an example for a single cell. Unbound (**D**) and bound (**E**) CD4 are pushed up from the glass surface (horizontal green dashed line, z_0) to the node plane (horizontal black dashed line) as shown in the plot of *z*-position as function of time (lower panels). Vertical cyan and red dashed lines indicate the start of the elevation (t_0) and the time of reaching a height of 8 µm (t_8), respectively. The dark blue line indicates the linear ramp of the acoustic amplitude. Most bound cells show mild elevation (2-3 mm) after t_0 under the acoustic pressure and only minimal *xy*-shifts. After bond rupture, cells move swiftly up to the node, while large *xy*-shifts are observed. The black dashed line indicates the threshold height above which a cell is considered unbound (z_0 + 8 µm). (**F**) z-position trajectories of an unbound, a binding and a bound CD4 during a typical bond-rupture measurement, with applied voltage indicated. The first 19 minutes are used to identify the cell state, also shown in **Figure 2A**. Subsequently a square-root amplitude ramp (14.3 MHz, 0-42 Vpp, 18 s) is performed, resulting in a linear force ramp (0-970 pN, 53.88 pN/s). The right panel is a zoom in of the amplitude ramp (indicated by the grey zone on the left), providing insight into the elevation of the cells, their residence in the acoustic node and their sedimentation to the bottom glass surface after switching of the acoustic waves.

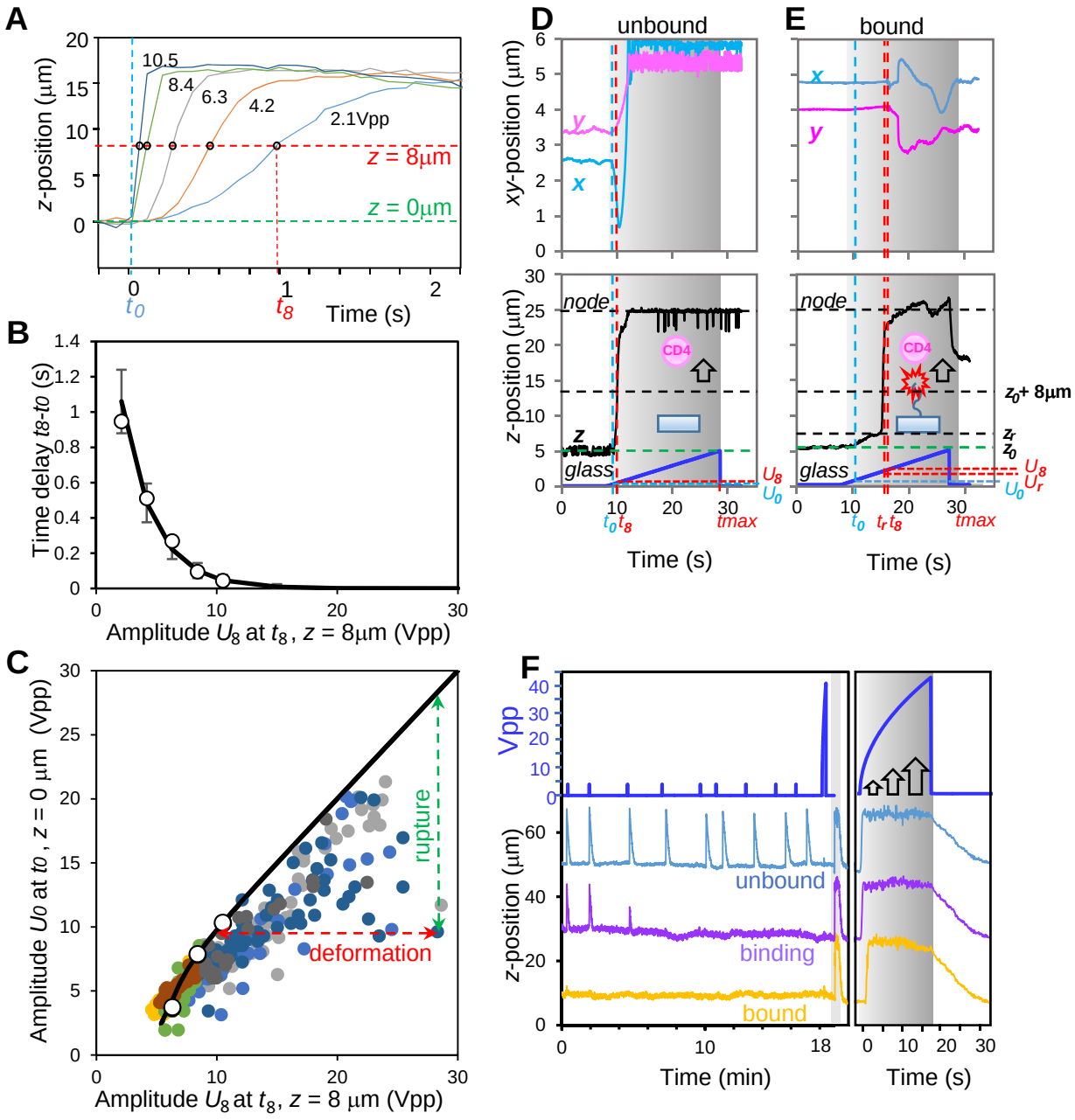

Figure S5: Determination of the exact rupture force of CD4, related to Figure 5.

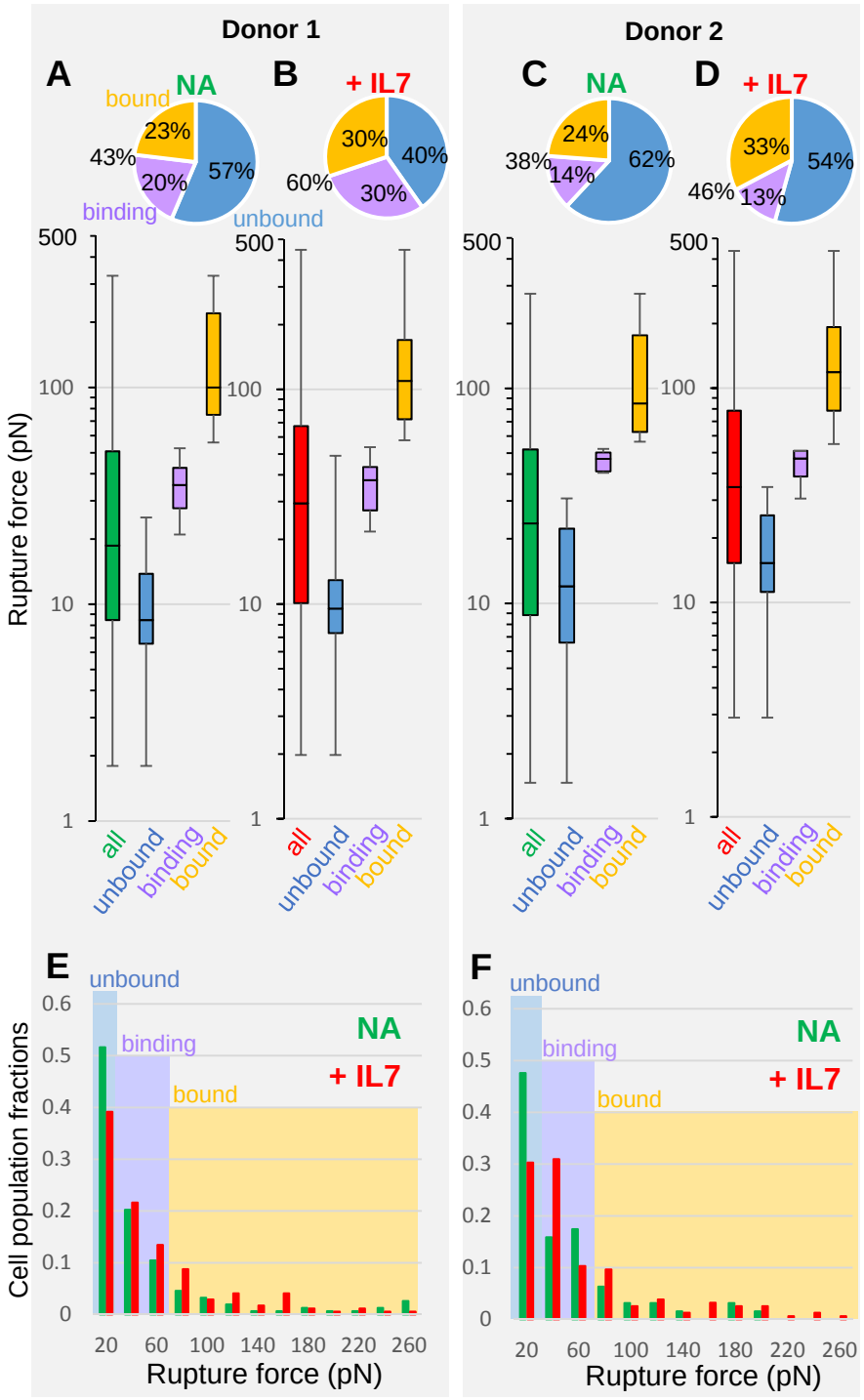

Figure S6: CD4 rupture-force measurements shown in Figure 3e, for both donors separately, related to Figure 6.

As shown in **Figure 5D**, an amplitude ramp of the acoustic wave (0-42V_{pp}) has been applied for 18 s to non-activated and IL7-activated cells after 19 min of incubation in the chamber. Pie charts give the proportions of unbound (blue), binding (purple) and bound (orange) cells for non-activated (**A/C**) and IL7-activated cells (**B/D**) for two representative blood donors. Box plots show the bond-rupture forces, Whiskers are maximum and minimum, and boxes indicate the second and third quartiles framing the median. (**E/F**) The bar graphs show the corresponding spectra of rupture forces of the representative donors. Cell percentages are given per slice of 20 pN of rupture force from 0 to 260 pN excluding the few high rupture force values (max 447pN). The unbound, binding and bound zones are indicated by blue, purple and orange, respectively.

1 Supplemental movie

Click here to access/download

Supplemental Videos and Spreadsheets

20171031Cell_SupMovie_SCAFS_Kamsma.avi